International Journal of Automotive Technology, Vol. 5, No. 4, pp. 247–255 (2004)

1229-9138/2004/018-03

DYNAMIC MODELING AND ANALYSIS OF VEHICLE SMART STRUCTURES FOR FRONTAL COLLISION IMPROVEMENT

A. M. ELMARAKBI* and J. W. ZU

Department of Mechanical and Industrial Engineering, University of Toronto, Toronto, Ontario, Canada, M5S 3G8

(Received 25 August 2003; Revised 17 August 2004)

ABSTRACT–The majority of real world frontal collisions involves partial overlap (offset) collision, in which only one of the two longitudinal members is used for energy absorption. This leads to dangerous intrusions of the passenger compartment. Excessive intrusion is usually generated on the impacted side causing higher contact injury risk on the occupants compared with full frontal collision. The ideal structure needs to have extendable length when the front-end structure is not capable to absorb crash energy without violating deceleration pulse requirements. A smart structure has been proposed to meet this ideal requirement. The proposed front-end structure consists of two hydraulic cylinders integrated with the front-end longitudinal members of standard vehicles. The work carried out in this paper includes developing and analyzing mathematical models of two different cases representing vehicle-to-vehicle and vehicle-to-barrier in full and offset collisions. By numerical crash simulations, this idea has been evaluated and optimized. It is proven form numerical simulations that the smart structures bring significantly lower intrusions and decelerations. In addition, it is shown that the mathematical models are valid, flexible, and can be used in an effective way to give a quick insight of real life crashes.

KEY WORDS : Crashworthiness, Full and offset frontal collision, Smart structures, Injury criteria, Numerical simulation

1. INTRODUCTION

Crashworthiness improvement and vehicle frontal collision mitigation have become one of the major research areas in automotive engineering. The increasing public awareness of safety issues and the increasing legislative requirements have increased the pressure on vehicle manufactures to improve the vehicle crashworthiness.

Most of real world frontal collisions involve partial overlap (offset) collision, in which only part of the vehicle structure can be used for energy absorption. This leads to dangerous intrusions of the passenger compartment, because only one of the two longitudinal members is used for energy absorption. Excessive intrusion is usually generated on the impacted side causing higher contact injury risk on the occupants compared with full frontal collision.

Excessive intrusion and higher risk of injuries are some of the tougher constraints to be satisfied when designing for offset crash. These constrains make it more challenging to seek an optimal design that maximizes the energy absorption capability, minimizes intrusion, and keeps occupant G-values within desired limits or less (Mahmood *et al.*, 1995).

*Corresponding author. e-mail: elmarak@mie.utoronto.ca

The ideal structure needs to have extendable length when the front-end structure is too short to absorb impact energy without violating deceleration pulse requirements. Moreover, the optimum structure for offset crash is to stiffen the impacted side of the structure, and to transfer part of the load to the non-impacted side to even out the load on both sides. A smart structure system has been proposed to meet these ideal requirements and to support the function of the existing vehicle structure. The proposed smart structure consists of two controlled hydraulic cylinders integrated with the front-end structure. The Proposed structure can be deployable prior to impact upon prediction of collision using radar collision prediction sensor. Deployable of the proposed structure has not been considered in this paper.

Frontal crashworthiness improvement using hydraulic cylinders was initially developed by Schwarz in (1971). In his research, hydraulic energy absorption systems were designed to mitigate high speed impacts up to 80 km/h. Moreover, using hydraulic cylinders to absorb crash energy at high speed collisions were investigated by Appel *et al.* (1973) to improve the crashworthiness of motor vehicles. The basic idea was tested by Rupp (1974). In his research, he utilized hydraulic buffers to maximize the absorbed impact energy. He used two

extendable, independently controlled hydraulic buffers integrated with the front-end longitudinal members. Rupp's study aimed to mitigate high-speed frontal impacts. Five different strokes were used and different impact speeds were investigated ranging from 36 km/h to 73 km/h. Recently, Jawad *el al.* (1999 & 2001) used hydraulic cylinders to mitigate high speed frontal impact. In their works, two controlled hydraulic cylinders were proposed to be extended prior to collision and absorb impact energy upon engagement with other body using radar collision prediction sensors. High speed collisions at 36 km/h, 56 km/h, and 64 km/h were investigated. Furthermore, Witteman *et al.* (1998 & 2001) used non extendable hydraulic cylinders improve the frontal impact at initial crash speed of 56 km/h. In addition, Witteman (1999) presented a study showing that increased protection for the entire collision spectrum can be obtained by a frontal structure consisting of two special longitudinal members. The longitudinal members are supported by a cable connection system for symmetric force distribution. Similar research by Clark (1994) presented another solution to improve vehicle frontal crashworthiness and to reduce the crash severity. In his work, he developed an extended airbag bumper system. With radar detection a collision is predicted and a large airbag deploys in front of the bumper.

In automotive industry, development of smart structures is continuously evolved by safety engineers. There are a few patents on smart structures since 1976 by Ellis (1976), Reube *et al.* (1994), and Wang (1994), which concentrate only on the design procedures. However, there is a lack of research with regard to the analysis of smart structures. The analysis of smart structures is powerful for redesign of systems to improve their performance. Furthermore, the analysis of smart structures facilitates the commercialization stage of the design.

This paper seeks to develop mathematical models of the smart structure in two different collision situations and to find numerical solutions to these models. A review of the previous work shows that little has been done for the development of simplified models for automotive crash problems in general, and smart structures in particular.

The development of such models is desirable to be used in the initial concept design stage of automotive structures before costly and time consuming large-scale finite element analysis is performed.

2. CRASHWORTHINESS ANALYSIS WITH LUMPED MASS MODELS

Mass-spring models are often applied in car research and development for car-to-car crashes, either in a simple form with a few masses or somewhat more complex form with about 50 masses (Coo *et al.*, 1991). Lumped mass models have been used since the early 1970s for the analysis and design of automotive structures for safety during crash (Kamal, 1970). In these models, the major undeformable structural components are represented by lumped masses and the major deformable structural components are modeled as nonlinear spring elements, typically represented with the force-deformation data obtained from experiments. Lumped parameter simulation has been employed for dynamic simulations and occupant analysis (Bennett *et al.*, 1991).

2.1. Mathematical Model of Frontal Collision

The simulation models presented in this paper are intended for different collision situations. Two different study cases representing vehicle-to- vehicle and vehicle -to-barrier in full and offset frontal collision are developed and analysed. It is worthwhile mentioning that vehicle components, which significantly affect the dynamics of frontal impact, are modelled by lumped masses and nonlinear springs. For the analysis of a vehicle structure that has to sustain a frontal collision, multiple aspects must be considered, i.e. collision velocity, crash direction, overlap percentage, and obstacle type, mass of the vehicle, etc. The energy dissipation in a frontal crash normally occurs by deformation of the longitudinal members. These must absorb a large part of the kinetic energy.

The model shown in Figure 1 represents two vehicles, denoted as vehicle 1, which indicates the standard vehicle and vehicle 2, which represents a vehicle with new front-end structure. They impact each other at initial velocities $(v_1)_o$ and $(v_2)_o$, respectively. The stiffness elements shown as springs, with stiffness k_{ij}, are the plastic deformation parts representing the longitudinal members. Dampers, with damping coefficient c_k represent the hydraulic cylinders.

The two bumpers' masses (bumper assembly) stay together after impact (perfectly plastic impact) and have a united velocity and displacement as shown in Figure 2.

The velocity of the bumper assembly is calculated using momentum equation of the two masses colliding head-on with zero coefficient of restitution.

In addition, the displacement of the bumper assembly is taken to be zero.

The masses of the bumper assembly and the cross member (to connect the hydraulic cylinders) are defined by m_b and m_{c2}, respectively.

The occupants restraint characteristics of seat belt and airbag are represented by stiffness k_{oi} and damping coefficient c_{oi}. Moreover, the masses of the vehicle body, engine, and occupant are represented by M_i, m_{Ei} and m_{oi}, respectively.

The following simplified assumptions are introduced

(1) Structural integrity of the passenger compartment is maintained throughout impact.

(2) The velocity is symmetric about its vertical central plane.

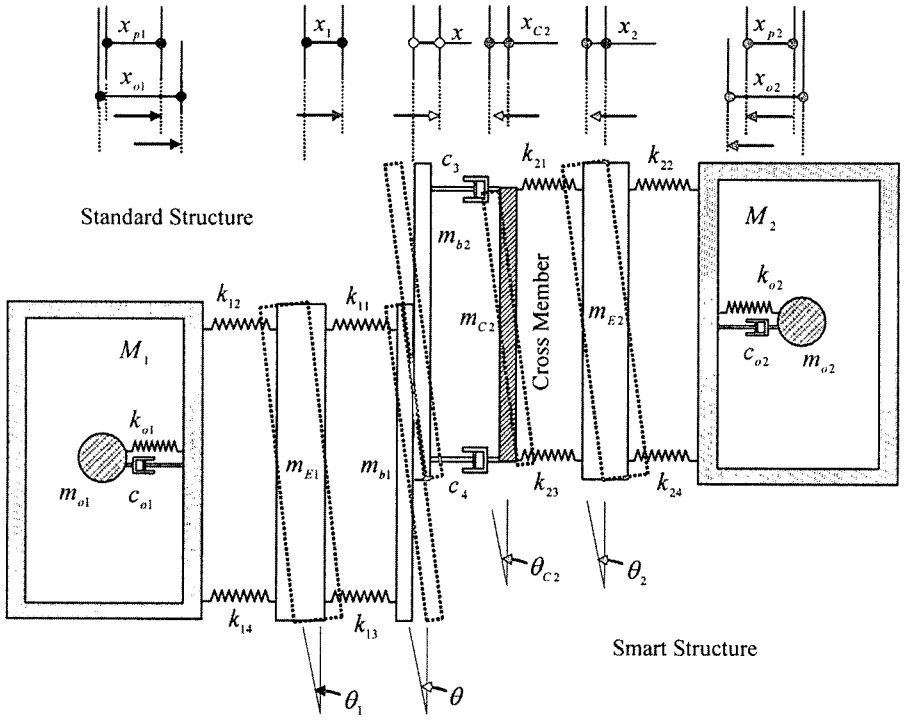

Figure 1. Mathemtical model of smart-standard vehicle in offset forntal collision.

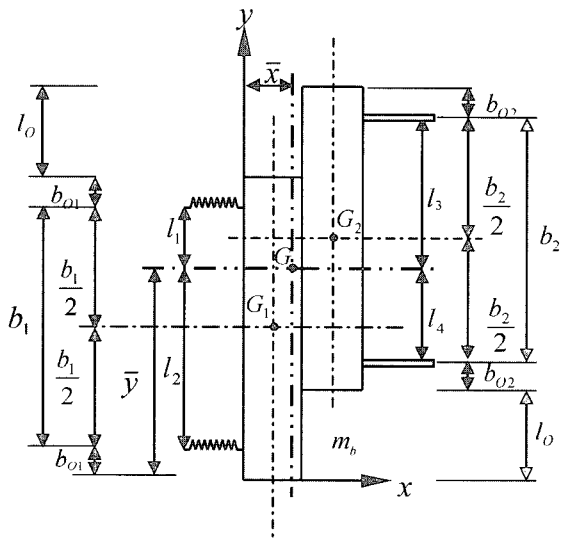

Figure 2. Mathematical model of the bumper assembly in offset frontal collision.

(3) The bumper assembly, cross member and engine are rotated in linear fashion.

Figure 3 shows the mathematical model of a smart vehicle-to-barrier in offset frontal collision. In addition, a standard vehicle-to-barrier collision can be simulated as a vehicle-to-vehicle collision of two identical vehicles with equal impact velocities.

2.2. Formulation

The initial collision event when a vehicle hits an obstacle (barrier, vehicle, etc.) is referred to as the first or primary collision. The following event when the occupant moves within the vehicle and impacts the interior is called the secondary collision.

2.2.1. Vehicle-to-vehicle primary collision

The equations of motion for the system shown in Figure 1can be derived as follows:

$$m_b \cdot \ddot{x} + F_{C3}(v_3) + F_{c4}(v_3) - F_{11}(\delta_{11}) - F_{13}(\delta_{13}) = 0 \quad (1)$$

$$m_{E1} \cdot \ddot{x}_1 + F_{11}(\delta_{11}) + F_{13}(\delta_{13}) - F_{12}(\delta_{12}) - F_{14}(\delta_{14}) = 0 \quad (2)$$

$$m_{C2} \cdot \ddot{x}_{C2} + F_{C3}(v_3) + F_{C4}(v_4) - F_{21}(\delta_{21}) - F_{23}(\delta_{23}) = 0 \quad (3)$$

$$m_{E2} \cdot \ddot{x}_2 + F_{21}(\delta_{21}) + F_{23}(\delta_{23}) - F_{22}(\delta_{22}) - F_{24}(\delta_{24}) = 0 \quad (4)$$

$$M_1 \cdot \ddot{x}_{p1} + F_{12}(\delta_{12}) + F_{14}(\delta_{14}) = 0 \quad (5)$$

$$M_2 \cdot \ddot{x}_{p2} + F_{22}(\delta_{22}) + F_{24}(\delta_{24}) = 0 \quad (6)$$

$$I \cdot \ddot{\theta} + F_{11}(\delta_{11}) \cdot l_1 + F_{C4}(v_4) \cdot l_4 - F_{C3}(v_3) \cdot l_3 - F_{13}(\delta_{13}) \cdot l_2 = 0 \quad (7)$$

$$I \cdot \ddot{x}_1 + (F_{12}(\delta_{12}) - F_{11}(\delta_{11})) \cdot (b_1 + b_{o1} - l_o) + (F_{13}(\delta_{13}) - F_{14}(\delta_{14})) \cdot (l_o - b_{o1}) = 0 \quad (8)$$

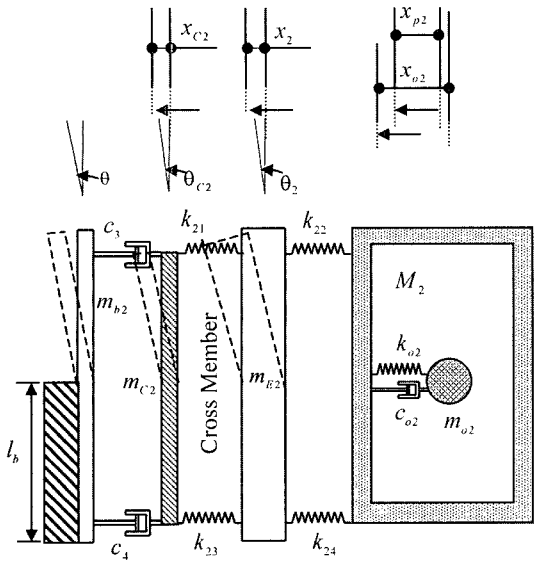

Figure 3. Mathematical mode of a smart vehicle-to barrier in offset frontal collision.

$$I_{C2} \cdot \ddot{\theta}_{C2} + (F_{C3}(v_3) - F_{21}(\delta_{21})) \cdot (l_o - b_{o2}) + (F_{23}(\delta_{23}) - F_{C4}(v_4)) \cdot (b_2 + b_{o2} - l_o) = 0 \quad (9)$$

$$I_2 \cdot \ddot{\theta}_2 + (F_{21}(\delta_{21}) - F_{22}(\delta_{22})) \cdot (l_o - b_{o2}) + (F_{24}(\delta_{24}) - F_{23}(\delta_{23})) \cdot (b_2 + b_{o2} - l_o) = 0 \quad (10)$$

2.2.2. Vehicle-to-barrier primary collision

The equations of motion for the system shown in Figure 3 can be derived as

$$m_{C2} \cdot \ddot{x}_{C2} + F_{C3}(v_3) + F_{C4}(v_4) - F_{21}(\delta_{21}) - F_{23}(\delta_{23}) = 0 \quad (11)$$

$$m_{E2} \cdot \ddot{x}_2 + F_{21}(\delta_{21}) + F_{23}(\delta_{23}) - F_{22}(\delta_{22}) - F_{24}(\delta_{24}) = 0 \quad (12)$$

$$M_2 \cdot \ddot{x}_{p2} + F_{22}(\delta_{22}) + F_{24}(\delta_{24}) = 0 \quad (13)$$

$$I \cdot \ddot{\theta} - F_{C3}(v_3) \cdot (b_2 + b_{o2} - l_b) = 0 \quad (14)$$

$$I_{C2} \cdot \ddot{\theta}_{C2} + (F_{C3}(v_3) - F_{21}(\delta_{21})) \cdot (b_2 + b_{o2} - l_b) = 0 \quad (15)$$

$$I_2 \cdot \ddot{\theta}_2 + (F_{21}(\delta_{21}) - F_{22}(\delta_{22})) \cdot (b_2 + b_{o2} - l_b) = 0 \quad (16)$$

2.2.3. Secondary collision

The equations of motion of the occupants can be written as follows:

$$m_{o1} \cdot \ddot{x}_{o1} + F_{o1}(\delta_{o1}) + F_{Co1}(v_{o1}) = 0 \quad (17)$$

$$m_{o2} \cdot \ddot{x}_{o2} + F_{o2}(\delta_{o2}) + F_{Co2}(v_{o2}) = 0 \quad (18)$$

where $\ddot{x}$, $\ddot{x}_i$, $\ddot{x}_{C2}$, $\ddot{x}_{pi}$ and $\ddot{x}_{o1}$ are the translation decelerations of the bumper assembly, engine, cross member, passenger compartment (vehicle body) and occupant, respectively.

$\ddot{\theta}$, $\ddot{\theta}_i$, $\ddot{\theta}_{c2}$, I, I_i and I_{c2} are the rotational decelerations and masses moment of inertia of the bumper assembly, engine and cross member, respectively.

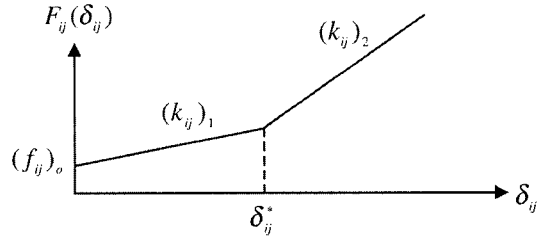

Figure 4. Force-deformation characteristic of the vehicle.

$F_{ij}(\delta_{ij})$ and $F_{ck}(v_k)$ are the forces of the plastic springs and damping forces, respectively.

$F_{oi}(\delta_{oi})$ and $F_{Coi}(v_{oi})$ are the forces generated on the occupant by springs and dampers of the restrained system, respectively.

2.3. Nonlinear Analysis

In case of crash analysis, the mass is always constant, while the damping and stiffness are not; they mainly depend on the velocity and displacement values. In this paper, the forces of the plastic springs $F_{ij}(\delta_{ij})$ and damping forces $F_{Ck}(v_k)$ are defined as

1–The forces generated by the plastic springs of the vehicle shown in Figure 4 are defined as

$$F_{ij}(\delta_{ij}) = (f_{ij})_o + (k_{ij})_1 \cdot \delta_{ij} \qquad \delta_{ij} \le \delta^*_{ij} \quad (19)$$

$$F_{ij}(\delta_{ij}) = (f_{ij})_o + (k_{ij})_1 \cdot \delta^*_{ij} + (k_{ij})_2 \cdot (\delta_{ij} - \delta^*_{ij}) \qquad \delta_{ij} > \delta^*_{ij} \quad (20)$$

where i=1,2 (i=1 represents vehicle 1, i=2 represents vehicle 2) and j=1,2,3,4 (represent vehicle's left, right, front and back rails).

2–The damping forces of the hydraulic cylinders shown in Figure 5 are expressed as follows:

$$F_{Ck}(v_k) = (c_k)_1 \cdot v_k \qquad v_k \le v^*_k \quad (21)$$

$$F_{Ck}(v_k) = (c_k)_1 \cdot v^*_k + (c_k)_2 \cdot (v_k - v^*_k) \qquad v_k \le v^*_k \quad (22)$$

where k=3, 4 (k=3 represents the right cylinder, k=4 represents the right cylinder).

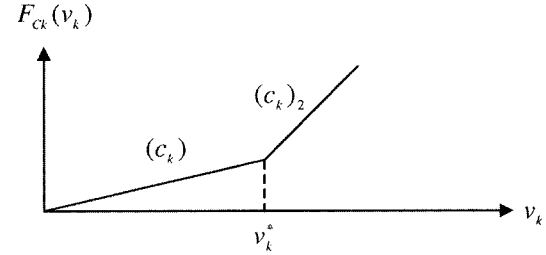

Figure 5. Force- velocity characteristic of the hydraulic cylinder.

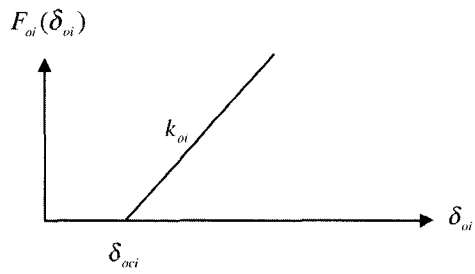

Figure 6. Force-deformation characteristic of the occupant.

3–The forces generated by the springs on the occupants shown in Figure 6 are given by

$$F_{oi}(\delta_{oi}) = 0 \quad \delta_{oi} \leq \delta_{oci} \tag{23}$$

$$F_{oi}(\delta_{oi}) = k_{oi} \cdot (\delta_{oi} - \delta_{coi}) \quad \delta_{oi} > \delta_{oci} \tag{24}$$

The damping coefficients on the occupants are taken as 20% of the critical damping as $c_{oi} = 0.4\sqrt{k_{oi}m_{oi}}$ and the damping forces on the occupant are determined as

$$F_{Coi}(v_{oi}) = 0 \quad v_{oi} \leq v_{coi} \tag{25}$$

$$F_{Coi}(v_{oi}) = c_{oi} \cdot (v_{oi} - v_{coi}) \quad v_{oi} > v_{coi} \tag{26}$$

where δ_{oci} is the initial slack length. The slack length represents the relative displacement of the occupant δ_{oi} before the seatbelt becomes effective. The relative velocity of the occupant when the seatbelt becomes effective is defined by v_{coi}.

The deformations of the plastic springs in the case of vehicle-to-vehicle collision are defined as follows:

$$\delta_{11} = x_{12} - x_{11} \tag{27}$$

$$\delta_{13} = x_{14} - x_{13} \tag{28}$$

$$\delta_{12} = x_{p1} - x_{12} \tag{29}$$

$$\delta_{14} = x_{p1} - x_{14} \tag{30}$$

$$\delta_{21} = x_{22} - x_{21} \tag{31}$$

$$\delta_{23} = x_{24} - x_{23} \tag{32}$$

$$\delta_{22} = x_{p2} - x_{22} \tag{33}$$

$$\delta_{24} = x_{p2} - x_{24} \tag{34}$$

$$\delta_{o1} = x_{o1} - x_{p1} \tag{35}$$

$$\delta_{o2} = x_{o2} - x_{p2} \tag{36}$$

The velocities of cylinders and occupants are given by

$$v_3 = \dot{x}_{21} + \dot{x}_{31} \tag{37}$$

$$v_4 = \dot{x}_{23} + \dot{x}_{41} \tag{38}$$

$$v_{o1} = \dot{x}_{o1} - \dot{x}_{p1} \tag{39}$$

$$v_{o2} = \dot{x}_{o2} - \dot{x}_{p2} \tag{40}$$

The displacements of the spring ends are expressed by

$$x_{11} = x - l_1 \cdot \tan\theta \tag{41}$$

$$x_{13} = x + l_1 \cdot \tan\theta \tag{42}$$

$$x_{21} = x_{C2} + (l_o - b_{o2}) \cdot \tan\theta_{C2} \tag{43}$$

$$x_{23} = x_{C2} - (b_2 + b_{o2} - l_o) \cdot \tan\theta_{C2} \tag{44}$$

$$x_{12} = x_1 - (b_1 + b_{o1} - l_o) \cdot \tan\theta_1 \tag{45}$$

$$x_{14} = x_1 + (l_o - b_{o1}) \cdot \tan\theta_1 \tag{46}$$

$$x_{22} = x_2 + (l_o - b_{o2}) \cdot \tan\theta_2 \tag{47}$$

$$x_{24} = x_2 - (b_2 + b_{o2} - l_o) \cdot \tan\theta_2 \tag{48}$$

$$x_{31} = x - l_3 \cdot \tan\theta \tag{49}$$

$$x_{41} = x + l_4 \cdot \tan\theta \tag{50}$$

The velocities of dampers ends are given by

$$\dot{x}_{31} = \dot{x} - l_3 \cdot \sec^2\theta\dot{\theta} \tag{51}$$

$$\dot{x}_{41} = \dot{x} + l_4 \cdot \sec^2\theta \tag{52}$$

$$\dot{x}_{21} = \dot{x}_{C2} + (l_o - b_{o2}) \cdot \sec^2\theta_C\dot{\theta}_C \tag{53}$$

$$\dot{x}_{23} = \dot{x}_{C2} - (b_2 + b_{o2} - l_o) \cdot \sec^2\theta_C\dot{\theta}_C \tag{54}$$

The deformations of the plastic springs in the case of vehicle-to-barrier collision are defined as Equations (31–34) and Equation (36). Morover, the velocities of hydraulic cylinder are given as

$$v_3 = \dot{x}_{21} - \dot{x}_{31} \tag{55}$$

$$v_4 = \dot{x}_{23} \tag{56}$$

The displacements of the spring ends are defined as

$$x_{21} = x_{C2} + (b_2 + b_{o2} - l_b) \cdot \tan\theta_{C2} \tag{57}$$

$$x_{23} = x_{C2} \tag{58}$$

$$x_{22} = x_2 + (b_2 + b_{o2} - l_b) \cdot \tan\theta_2 \tag{59}$$

$$x_{24} = x_2 \tag{60}$$

$$x_{31} = (b_2 + b_{o2} - l_b) \cdot \tan\theta \tag{61}$$

$$x_{41} = 0 \tag{62}$$

The velocities of dampers ends are given by

$$\dot{x}_{21} = \dot{x}_{C2} + (b_2 + b_{o2} - l_b) \cdot sec^2\theta_C\dot{\theta}_C \tag{63}$$

$$\dot{x}_{23} = \dot{x}_{C2} \tag{64}$$

where x, x_i, x_{C2}, x_{pi} and x_{oi} are the translation displacements of the bumper assembly, engine, cross member, passenger compartment (vehicle body) and occupant, respectively.

$\dot{x}$, $\dot{x}_i$, $\dot{x}_{C2}$, $\dot{x}_{pi}$ and $\dot{x}_{oi}$ are the translation velocities of the bumper assembly, engine, cross member, passenger compartment (vehicle body) and occupant, respectively.

θ, θ_i, θ_{C2} are the angles of rotation of the bumper assembly, engine, cross member, respectively.

θ, θ_i, θ_{C2} are the rotational velocities of the bumper assembly, engine, cross member, respectively.

3. INJURY SEVERITY CRITERIA

To compare the injury severity for different vehicle collisions, some kind of index or formula is needed. The main injury criterion of interest in this paper is the intrusion criterion, which denotes the interior deformation of the vehicle structure and its effects on the passenger compartment. High impact speeds may result in more severe injuries to vehicle occupants. The intrusion levels depend on how the vehicle structure is assembled and how the impact energy is absorbed by the vehicle structure. The second injury criterion that has been considered is the deceleration level of the occupant.

The injury criteria will be used for interpreting the results of the simulation. The intrusion injury criterion measured as the maximum deformation suffered by the back rail. Moreover, deceleration injury criterion measured as the maximum deceleration pulse sustained by occupant during the crash.

4. SIMULATIONS

Numerical simulations are used as a tool to demonstrate the influence of various crash situations on the energy absorbed by the proposed structure. The finite difference method is used to solve the differential Equations (1-18). The initial conditions are specified as

$$x(0) = x_1(0) = x_2(0) = x_{C2}(0) = x_{p1}(0) = x_{p2}(0) = x_{o1}(0) = x_{o2}(0) = 0 \quad (65)$$

$$v_1(0) = v_{p1}(0) = v_{o1}(0) = (v_1)_0 \quad (66)$$

$$v_2(0) = v_{C2}(0) = v_{p2}(0) = v_{o2}(0) = (v_2)_0 \quad (67)$$

The following data are used in the numerical solution. The mass of the vehicle body is M_i=1200 kg, the mass of the engine is m_{Ei}=300 kg, the mass of the bumper assembly is m_b=100 kg and the mass of the cross member is m_{C2}=20 kg.

In addition, the force-deformation characteristic for each longitudinal rail is shown in Figure 4 with the following values: $(k_{ij})_1$=400 kN/m, $(k_{ij})_2$=500 kN/m with d_{ij}^*=0.20 m for the front rail and $(k_{ij})_1=(k_{ij})_2$=900 kN/m with $(f_{ij})_o$=80 kN for the back rail. The damping coefficient $(c_k)_1$ is taken to be 1.0 kN·s/m with v_k^*=10 m/s, and $(c_k)_2$=1.5 kN·s/m for each cylinder. The mass of the occupant is m_{oi}=65.7 kg.

Morover, the occupants restrained characteristics of seat belt and airbag are represented by stiffness is k_{oi}=98.1 kN/m with δ_{oci}=0.01 m and damping coefficient is c_{oi}=20% of the critical damping. The initial velocity of the vehicle and the occupant is v_o=13.33 m/s.

4.1. Vehicle-to-Vehicle Collision

4.1.1. Full collision

The fundamental advantage of the ability of smart structures is to absorb more energy for the same crush distance and for the same maximum load level. This is achieved by the ability of smart structures to use more distance available for crush which otherwise is occupied by the folded material of standard structures. The aim of this investigation is to demonstrate the performance of the smart structure in full frontal collisions. Two sets of simulation runs involving two vehicles in head-on collision are used. The first set (smart collision) involves a collision of the smart vehicle (SM) with the standard vehicle (ST). The second set (standard collision) involves a collision of the two identical standard vehicles. The hydraulic cylinder is extended by 0.4 m. Figures 7 and 8 compare the deformation of the back rail and the deceleration of the occupant of two set-ups respectively.

Figure 7 clearly shows the significant reduction in the intrusion injury in full frontal collision. This can be concluded by noting that the smart vehicle produced 0.25 m back rail deformation of the impacted side, compared to 0.29 m of the partner vehicle while in the standard collision, the impacted back rail is deformed by 0.33 m. It is clear from Figure 8 that the smart vehicles occupant suffers lower deceleration (35 g). Moreover, the smart structure reduces the deceleration of the partner vehicles

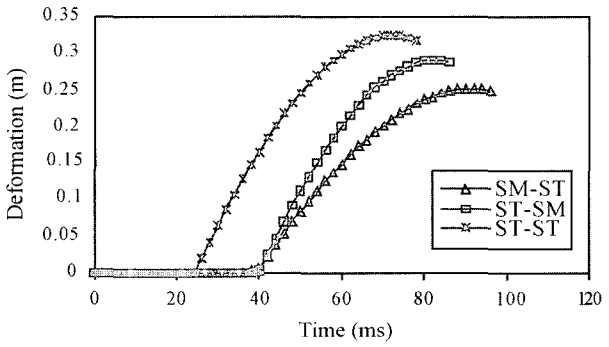

Figure 7. Deformation of the back rail full collision.

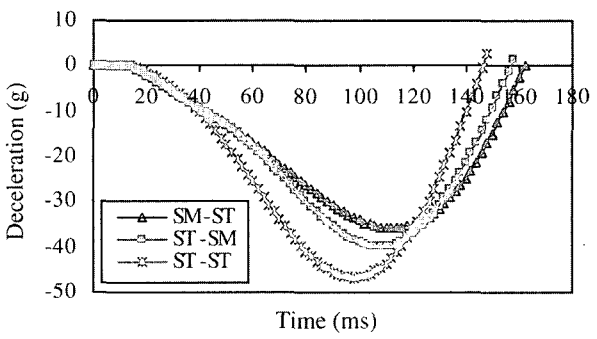

Figure 8. Deceleration of the occupant- full collision.

occupant to 40 g while in the standard collision; the occupant sustains more deceleration (47 g).

4.1.2. Offset collision

Likewise, the aim of this simulation is to compare the performance of the proposed vehicle structure in 50% offset frontal collisions. Two sets of simulation runs involving two vehicles in head-on collision are used. The first set (smart collision) involved a collision of the smart vehicle (SM) with the standard vehicle (ST). The second set (standard collision) involved a collision of the two identical standard vehicles. Figures 9 and 10 compare the deformation of back rail and the deceleration of the occupant of two set-ups respectively. The same results are also gained in 50% offset frontal collision for both sets of simulations.

Figure 9 clearly shows the energy absorption feature of the smart structure by noting that the smart vehicle minimizes the intrusion for both vehicles. It can be concluded by noting that the smart vehicle produced 0.44 m back rail deformation, compared to 0.46 m of the partner vehicle while in the standard collision, the impacted back rail is deformed by 0.55 m.

The result of the second injury criteria, deceleration of the occupant, is depicted in Figure 10. It shows that the smart vehicles occupant sustains lower deceleration (21 g). Moreover, the smart structure reduces the deceleration of the partner vehicles occupant to 24 g while in the standard collision, the occupant suffers more deceleration (27 g).

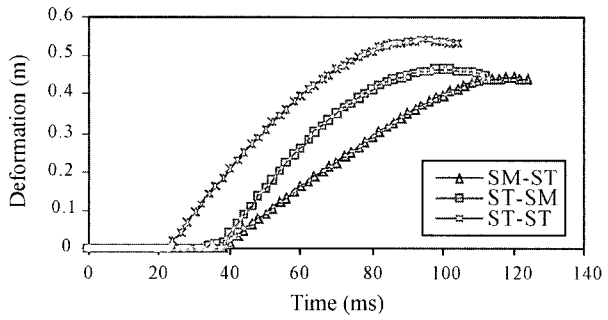

Figure 9. Deformation of the back rail- offset collision.

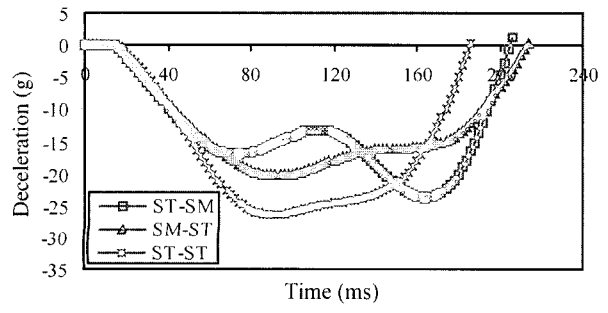

Figure 10. Deceleration of the occupant-offset collision.

4.2. Vehicle-to-Barrier Collision

Vehicle-to-barrier collision is generally accompanied by high intrusion and is usually more critical than vehicle-to- vehicle collision. Two sets of simulation run involving vehicle-barrier in head-on collision are used. The first set (smart collision) involves a collision of the smart vehicle (SM) with a fixed rigid barrier. The second set (standard collision) involves collision of the standard vehicle (ST) with the fixed barrier. In addition, two different simulations for two different collision events (full and 50% offset frontal collision) are conducted.

4.2.1. Full collision

The time-histories of the back rail deformation and the deceleration of the occupant, as obtained from the two simulations, are shown in Figures 11 and 12 respectively. The reduction of the back rail deformation is clearly shown in Figure 11. The back rail of the smart structure is deformed by 0.27 m, compared to 0.33 m of the standard vehicle.

Furthermore, Figure 12 shows that the peak amplitude of the deceleration of the smart vehicles occupant appears to be about 38 g. While the corresponding value of the standard vehicles occupant is 47 g, which is significantly higher.

4.2.2. Offset collision

The goal of this simulation is to compare the performance

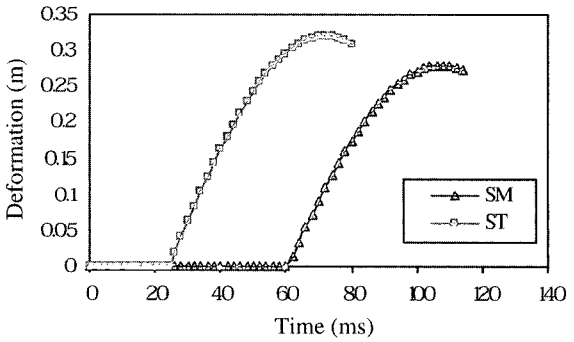

Figure 11. Deformation of the back rail-full collision.

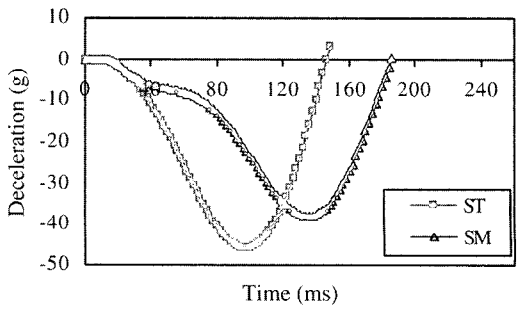

Figure 12. Deceleration of the occupant- full collision.

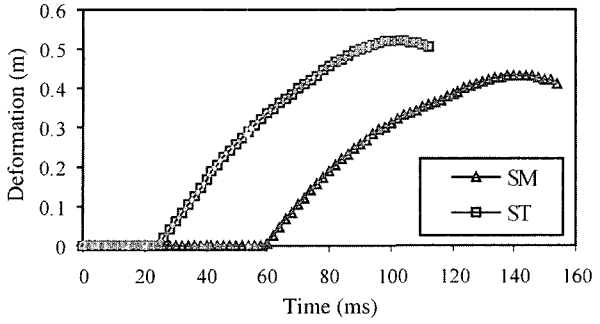

Figure 13. Deformation of the back rail- offset collision.

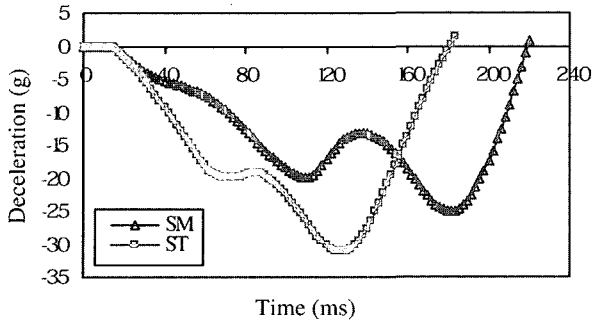

Figure 14. Deceleration of the occupant- offset collisions.

of the smart structure in 50% offset barrier collision which represents the more likely case in vehicle -to-barrier collisions. Two different simulations for standard and smart vehicle offset barrier collision are conducted. The time-histories of the back rail deformation and the deceleration of the occupant are obtained from the simulations and depicted in Figures 13 and 14, respectively.

Figure 13 clearly shows the maximum back rail deformation of the impacted side of the vehicle. it is worthwhile noting that the smart vehicle's back rail deformed by 0.43 m, compared to 0.53 m of the standard vehicle. the peak amplitude of the deceleration of the standard vehicle's occupant appears from figure 14 to be about 25 g, compared to 31 g of the smart vehicle's occupant.

5. CONCLUSION

The improved frontal crashworthiness of vehicles necessitates totally new design concepts which take into account that the majority of collisions occur with partial frontal overlap. To adapt structure design for crash conditions, offset crashes ideally require stiffer structure on the impacted side and softer structure on the other side. A novel system is introduced to support the function of the existing vehicle structure. The proposed structure consists of two independently controlled hydraulic cylinders integrated with the front-end longitudinal members. Two different cases of spring-mass-damper mathematical models representing vehicle-to-vehicle, and vehicle-to-barrier in full and offset collisions are investigated. Numerical simulations prove that the smart structure concept surpasses the traditional structure concept in absorbing crash energy for the same crash distance. Furthermore, it is shown that the mathematical models are valid, flexible and can be useful in optimization studies.

REFERENCES

Appel, H. and Tomasd, J. (1973). The enrgy management structure for the Volkswagen ESV. *SAE Paper No.* 730078.

Bennett, J., Lust, R. and Wang, J. (1991). Optimal design strategies in crashworthiness and occupant protection. *The ASME Mechanical Engineering Congress and Exposition*, New York, USA, 51–66.

Clark, C. (1994). The crash anticipating extended airbag bumper system. *14th ESV Conference*, Munich, Germany, 1468–1480.

Coo, P., Janssen, E., Goudswaard, A., Wismans, J. and Rashidy, M. (1991). Simulation model for vehicle performance improvement in lateral collision. *13thESV Conference*, Paris, France, *Paper No.* 91-S5-O-25.

Ellis, E. (1976). Extensible vehicle bumper, *US Patent Office, Pat No.* 3947061.

Jawad, S., Mahmood, H. and Baccouch, M. (1999). Smart structure for improving crashworthiness in vehicle frontal collisions. *The ASME Mechanical Engineering Congress and Exposition*, Nashville, Tennessee, USA, 135–144.

Jawad, S. and Baccouch, M. (2001). Frontal offset crash-smart structure solution. *The ASME Mechanical Engineering Congress and Exposition*, New York, NY, USA, 213–222.

Kamal, M. (1970). Analysis and simulation of vehicle-to-barrier impact. *SAE Transactions*, **79**, *SAE Paper No.* 700414.

Mahmood, H., Baccouch, M. and Bakkar, J. (1995). Designing for offset crash: a trade-off in constraints. *SAE Paper No.* 951075.

Reuber, G. and Braun, A. (1994). Bumper system having an extendable bumper for automotive Vehicles. *US Patent Office, Pat No.* 5370429.

Rupp, W. (1974). Front energy management parametric variation study. *5th ESV Conference*, London, England, 602–614.

Schwarz, R. (1971). Hydraulic energy absorption systems for high-energy collisions. *2nd ESV Conference*, Sindelfingen, Germany, Sec. **3**, 36–74.

Wang, J. (1994). Bumper energy absorber. *US Patent Office, Pat No. 5967573.*

Witteman, W. and Kriens, R. (1998). Modeling of an

innovative frontal car structure: similar deceleration curves at full overlap, 40 percent offset and 30 degrees collisions. *16th ESV Conference*, Windsor, Ontario, Canada, 194–212.

Witteman, W. (1999). Improved vehicle crashworthiness design by control of the energy absorption for different collision situations. *Ph.D. Dissertation*. Eindhoven University of Technology, Automotive Engineering & Product Design Technology, Eindhoven, The Netherlands.

Witteman, W. and Kriens, R. (2001). The necessity of an adaptive vehicle structure to optimize deceleration pulses for different ceash velocities. *17th ESV Conference*, Amsterdam. The Netherlands. 1–10.